

Fiber–matrix interface – information from experiments via simulation

George N. Frantziskonis

Department of Civil Engineering & Engineering Mechanics, University of Arizona, Tucson, AZ 85721, USA

Prasanna Karpur

Research Institute, University of Dayton, 300 College Park Avenue, Dayton, OH 45469-0127, USA

Theodore E. Matikas

NRC Associate, WL/MLLP, Materials Directorate, Wright Laboratory, Wright-Patterson Air Force Base, OH 45433-7178, USA

S. Krishnamurthy

Universal Energy Systems, Inc., 4401 Dayton-Xenia Rd, Dayton, OH, USA

&

Paul D. Jero

Wright Laboratory, Materials Directorate, WL/MLLM, Wright-Patterson Air Force Base, OH 45433-6533, USA

This study explores a novel procedure for obtaining quantitative information on the mechanical properties of the fiber–matrix interface in composite materials. The method, based on lattice discretization of a medium, simulates actual experiments in detail, including fiber breakage, matrix yield and/or cracking, and interface failure. The paper concentrates on two experiments performed commonly, the so-called fragmentation test for metal matrix, and the pushout/pullout test for metal as well as ceramic matrix composites. Based on the documented capability of the method to simulate actual experimental data, reliable values of (homogenized) interface properties can be obtained. In addition, the simulations provide further understanding of the mechanisms involved during the relevant testing. Although this study presents results from basic problems, the method is general enough to include effects of residual stress, of high temperature environment, and of dynamic crack propagation, as well as three-dimensional details of the interface failure process. The potential exists for simulating nondestructive wave-based techniques aimed at evaluating interface properties.

1 INTRODUCTION

Physical reasoning and relevant research, i.e. Kerans *et al.*¹ and Evans and Marshall,² suggest that the mechanical properties of composite materials rely significantly on the nature of the interface between fiber reinforcement and matrix. It is the interface that delivers information (kinematic and dynamic quantities) from the matrix to the fiber and vice versa. Failure of composites involves not only failure of fibers and matrix, but also the propagation of cracks along and across, as explained subsequently, interfaces. The characteristics of such cracks, i.e. dissipated energy

during propagation, their interplay with matrix/fiber, etc., are decisive for the macroscopic properties of a composite. It is therefore important to understand the interface properties and their role in the overall mechanical performance of a composite. Consequently, interfacial characterization has received intensive attention, from the experimental as well as the analytical point of view.

Various experimental procedures addressing interfacial properties have been designed. Mechanical destructive tests have been and are being used, i.e. Jero *et al.*³ and Parthasarathy *et al.*⁴ Recently, attempts to characterize interfacial properties nondestructively have also been exa-

mined by Karpur *et al.*⁵ It is not intended herein to provide a thorough review of the literature on interfacial properties and testing. However, reference is given to those works directly relevant to the present study. For reviews and trace of the literature we refer to Metcalfe⁶ and Evans *et al.*⁷ and the works cited therein. For analysis of micro-mechanical stresses involved we refer to McCartney⁸ and Pagano.⁹

In general, a 'universal' experimental procedure designed to identify interface properties for various material combinations has not been identified. This is due to the fact that it is very difficult, if not impossible, to examine interface properties directly, to isolate the interface response. The relevant test measurements are sensitive to the properties of the matrix, the fiber(s), the interface(s) present, and the geometry and load conditions of the test setup. For example, while the so-called single fiber fragmentation (SFF) test has been used extensively for studying polymer, and lately metal matrix composites (MMCs), there are still a number of questions concerning the applicability of this test to evaluate interface strength. The SFF test is inappropriate for ceramic matrix composites (CMCs), as discussed further in the following.

The present study focuses on (a) the single fiber fragmentation test, often performed on metal matrix composites, and (b) on the pushout and pullout tests on metal and ceramic matrix composites. The following section concentrates on the information available from such tests, and is followed by the description of the numerical simulation procedure used herein, and presentation of relevant results. Throughout, the paper discusses the method and results, and the potential of the approach. It is stressed that more needs to be understood in this important area of interface properties identification. It seems that success in doing so depends heavily on close cooperation between those doing experimental work, both destructive and non-destructive, and those doing analytical, simulation work.

2 EXPERIMENTAL INFORMATION

In the SFF test a fiber is embedded in a ductile matrix (the applicability of the test to composites with limited ductility matrices is currently being considered). The sample is subjected to tensile loading along the fiber axis. Through transfer of load from the matrix to the fiber, at some point of

loading the fiber breaks. Further loading results in the fiber breaking into successively smaller fragments until the fragments become too short to enable further increase in the fiber stress level. Figure 1 (from Roman *et al.*¹⁰ where also an overview on the single fiber fragmentation test is given) contains typical results obtained from fragmentation tests on SCS-6 SiC fiber with Ti-6Al-4V and Ti-14Al-21Nb (wt%) matrix. According to Roman *et al.*¹⁰ the Ti-6Al-4V matrix possesses enhanced ductility and shows continuous yielding without yield drop or shear band or localized deformation zone formation. The Ti-14Al-21Nb shows a much more complicated response at post-yield strains.

Fiber fragmentation can be studied nondestructively. For example, a difference in the fiber fragmentation behavior between Ti-6Al-4V and Ti-14Al-21Nb composites with SCS-6 SiC fiber has been observed at room temperature by Karpur *et al.*^{11,12} as shown in Fig. 2. From cross-sectional photomicrographs of these composite systems, it is apparent that the Ti-6Al-4V shows a greater degree of chemical bonding (and the resulting mechanical bonding due to the interface roughness) compared to that of Ti-14Al-21Nb which shows a smooth interface. The fiber fragmentation of these two composite systems (Fig. 2) shows a corresponding shorter fragmentation size in Ti-6Al-4V compared to Ti-14Al-21Nb.

This study concentrates on the Ti-6Al-4V matrix. As shown in Fig. 1 the specimen shows a significant amount of plastic deformation. Since the acoustic emission bursts correspond mainly to fiber fracture,¹⁰ it is seen that fiber fragmentation initiates after the matrix (Ti-6Al-4V) has reached its yield stress. This information is important for identifying interface properties as shown subsequently.

Fragmentation tests are often performed on metal matrix as well as polymer matrix composites. The multiple fracture behavior has been studied mostly through the so-called shear lag analysis which provides a relation among the critical aspect ratio of the fiber, the tensile strength of the fiber, and the interfacial shear stress. Using arguments based on shear lag analysis, Kelly and Tyson¹³ showed that the critical length of fiber for load transfer, L_c , is a function of the interfacial shear stress according to the equation $\tau_i = \sigma_t d / 2L_c$ where τ_i is the shear stress, σ_t is the tensile strength of the fiber of critical length and d is the fiber diameter. Several limitations of the method have been identified. The method neglects the

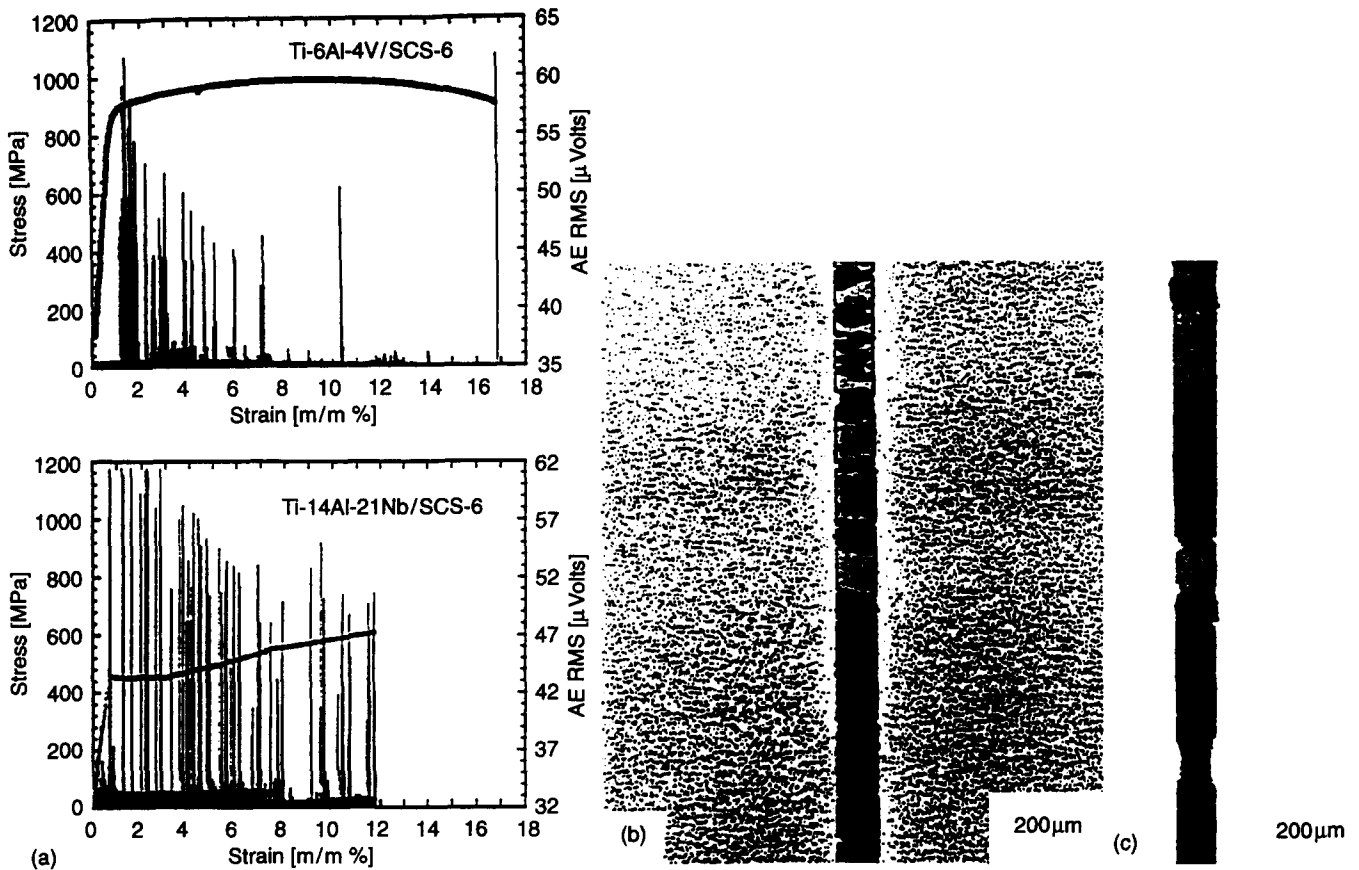


Fig. 1. (a) Typical tensile stress-strain curves and acoustic emission RMS-strain plots for two single fiber composite systems at room temperature. (b), (c) Optical micrographs showing a portion of the fragmented fiber in the two composites after tensile testing: (b) Ti-6Al-4V, (c) Ti-14Al-21Nb matrices, SCS-6 fiber. After Roman *et al.*¹⁰

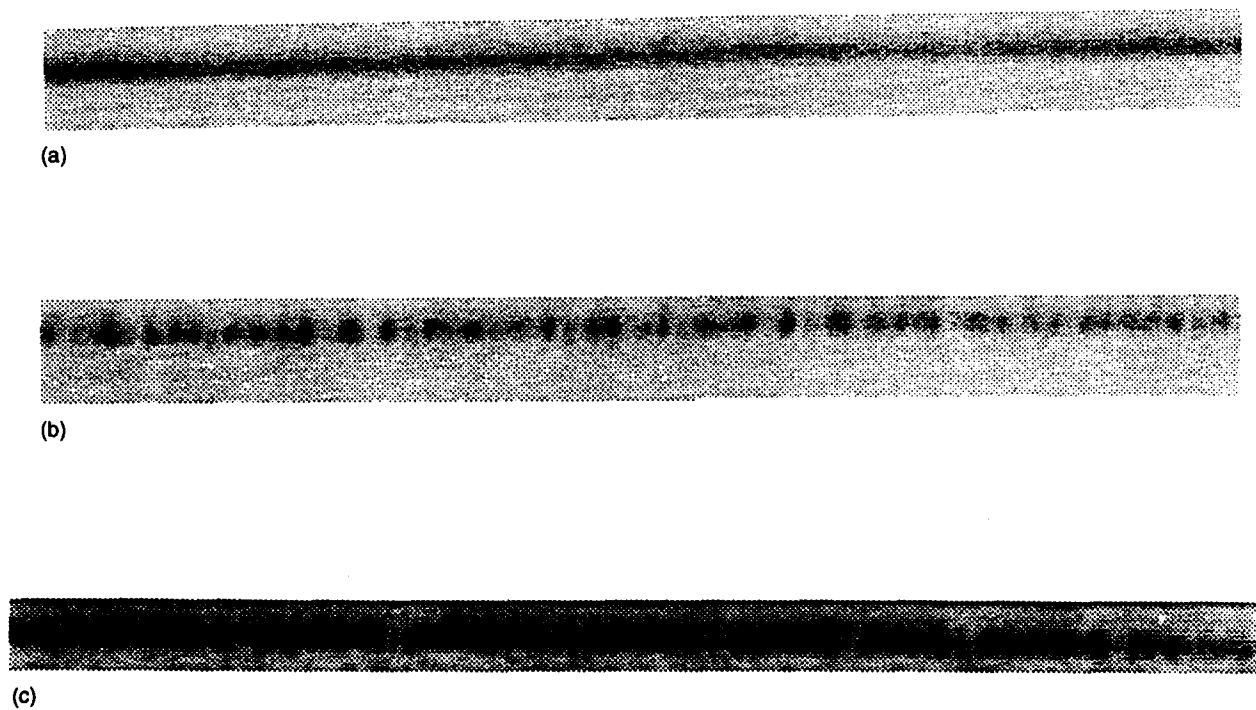


Fig. 2. Typical images obtained nondestructively using oblique incident ultrasonic shear waves of 25 MHz frequency: (a) from an untested sample with single SCS-6 fiber embedded in titanium aluminide matrix; (b) from Ti-6Al-4V/SCS-6 sample after loading, showing the fiber breaks approximately one fiber diameter long; (c) from Ti-14Al-21Nb/SCS-6 sample after loading, showing the fiber breaks approximately three fiber diameters long.

dependence of the interfacial shear stress on the volume and strain hardening characteristics of the matrix, the modulus of the matrix, and the strengths of fiber and matrix. Also, the interfacial characteristics predicted by that method are often very unrealistic.¹⁰ Ochiai and Osamura^{14,15} have attempted to overcome some of the limitations of the shear lag analysis by considering the details of stress transfer (from matrix to fiber) and plastic stress-deformation response for the matrix. They have also reported numerical results by assigning a Weibull distribution to the fiber spatial strength.

The so-called pushout and pullout tests are commonly performed on ceramic and metal matrix composites. Figure 3 shows a typical configuration for a pushout test. For fiber pullout, tensile load is applied on the fiber. For the numerical simulations described in the next section we consider pushout and pullout of a SiC (Textron SCS-6) fiber embedded in a Ti-6Al-4V matrix, and in a glass matrix. The length of the fiber pushed out in metal matrix is much shorter than the length in ceramic matrix composites. This is mostly due to experimental difficulties in testing long fiber lengths in a metal matrix. As shown herein, these geometrical differences have important consequences on the information obtained from the tests.

The literature on the pushout and pullout test is rich. For a review of the reported experimental, analytical work in this area we refer to Kerans and Parthasarathy¹⁶ for ceramic matrix and to Watson and Clyne^{17,18} for metal matrix composites. A large number of parameters influence the results from such tests, i.e. non-uniformities due to end effects, residual (radial and axial) stresses, the stability of interface crack propagation, and the elastic properties of the fiber and matrix. Relevant analytical works examine some of the underlying mechanisms, the result being a better understanding of the problem.¹⁶⁻¹⁹

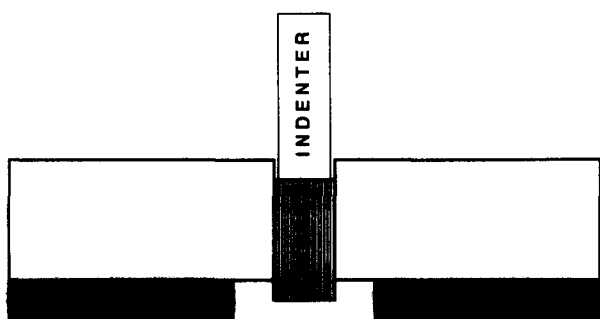


Fig. 3. Schematic of pushout test.

3 SIMULATIONS

Mechanics of materials research has been traditionally carried out through experiments and theoretical analysis. Recently, however, a new trend of computer-assisted research has evolved. This branch has been triggered by the rapid progress in computer performance, and from the increasing need for the understanding of systems far more complex than traditional techniques have ever handled. For example, in a typical single fiber fragmentation test, one can identify many complicated processes that take place concurrently — matrix yielding, fiber failure, interface failure and transfer of stress through the interface and matrix. It is important that such processes are understood so that the role of the interface can be identified and quantified.

In order to simulate such problems numerically, one may automatically think of the finite element method (FEM). However, within the FEM framework it is difficult to simulate the fracture processes occurring at the microlevel (at the length scale of a material's microstructure). Such a process would require use of elements much smaller than the crack sizes and significant mesh refinement, in addition to the requirement for a continuum-based fracture criterion (at the microlevel) that may be difficult to specify.

In this work, a microscopic representation of the fiber, matrix and interface is achieved through a so-called lattice. Lattices are being used extensively in different scientific fields, i.e. fluid mechanics, physics, etc., particularly as a tool to solve differential equations. Such a method for solution of problems within linear elasticity was, apparently, first investigated by Hrennikoff.²⁰ There it is shown that a lattice provides a consistent approach to the solution of elasticity problems — the solution converges to the exact elasticity solution with lattice spacing reduction. The advantages of using a lattice (over FEM) become evident (as further explained in the sequence) when (micro) fracturing is important. Such advantages have been realized by a branch of statistical physics where micro-fracturing in statistically heterogeneous solids is examined extensively.^{21,22} A number of works simulating the process of micro-fracturing in composite materials using a lattice discretization have been reported in the literature recently. It seems that this approach is receiving increasing attention: see the works of Schlangen and van Mier²³ in modeling microcracking in cement-base composites, of

Murat *et al.*²⁴ and Monette *et al.*²⁵ in modeling the behavior of short fiber reinforced composites, and of Dai and Frantziskonis²⁶ in modeling the statistical fracturing of cementitious composites and correlating it with ultrasonic nondestructive measurements.

In this study we utilize a triangular lattice. The properties of the unit cell are, for the case of linear, isotropic elasticity, as follows: Young's modulus equal to the modulus assigned to the bonds of the unit cell, and a Poisson ratio that depends explicitly on the (constant) angular stiffness between bonds. Angular refers to the rotational stiffness between adjacent bonds. In the absence of angular stiffness the Poisson ratio of the unit cell is equal to $1/3$. For a thorough presentation of the lattice properties and different lattice types we refer to Hrennikoff,²⁰ Herrmann and Roux,²¹ Murat *et al.*²⁴ It is also possible, without extensive effort, to consider anisotropy within a unit lattice cell, nonlinear effects, etc. Also, by assigning beam bending stiffness to the bonds, micro-rotational (Cosserat) effects are recovered. However, in this study we consider the simplest possible case, which calls for a triangular lattice without angular stiffness. Besides simplicity, the following advantages can be identified. Since interest is on fracture at the unit cell level, using such a lattice there is only one choice to serve as bond-failure criterion, namely the level of stress or the level of the corresponding strain at a bond. This is important since it is very difficult to identify (experimentally) the local conditions under which failure at the micro-level occurs. Since in a composite material properties vary spatially (i.e. transition from matrix to interface to fiber) ambiguities related to the angular stiffness at the transition zones — that may render the problem non-unique — are not present when using a 'central force' lattice. On the other hand, the Poisson ratio of $1/3$ may not be precise. For the material combinations considered herein such a value is not unreasonable for the matrices. For the fiber, the problem of Poisson ratio determination is a difficult one and rigorous methods for its determination have not been established. Furthermore, it is very difficult to determine (experimentally) the local characteristics (i.e. Poisson ratio) of interfaces/interface reaction zones.

In short, there are several issues to be resolved before an accurate representation of Poisson, local anisotropy, length scales, and perhaps local rotational (Cosserat) effects come into the picture. Thus we proceed in this study by considering the

simplest possible case, the central force triangular lattice throughout the domain of interest.

3.1 The interface

Figure 4 shows a 40×120 triangular lattice, which is one of the lattices used for simulating the single fiber fragmentation test. The fiber is placed in the center of the lattice in Fig. 4, parallel to the y -direction, and together with the interface is considered to be four lattice spacings wide and 94 spacings long (4×94). The rest of the lattice is assigned matrix properties, and a single lattice spacing is assigned interface properties. From a first evaluation it may seem that the interface region considered is too 'thick'. This brings up the problem of interface thickness, and, as will be explained, there is a simple way to account for this in the analysis.

As far as terminology is concerned, the term 'transition region' (*cf.* the following discussion) may be more appropriate than 'interface'. A transition region allows elastic deformation within the 'interface' before fracture. However, both terms are used in the following, hoping that confusion is not possible.

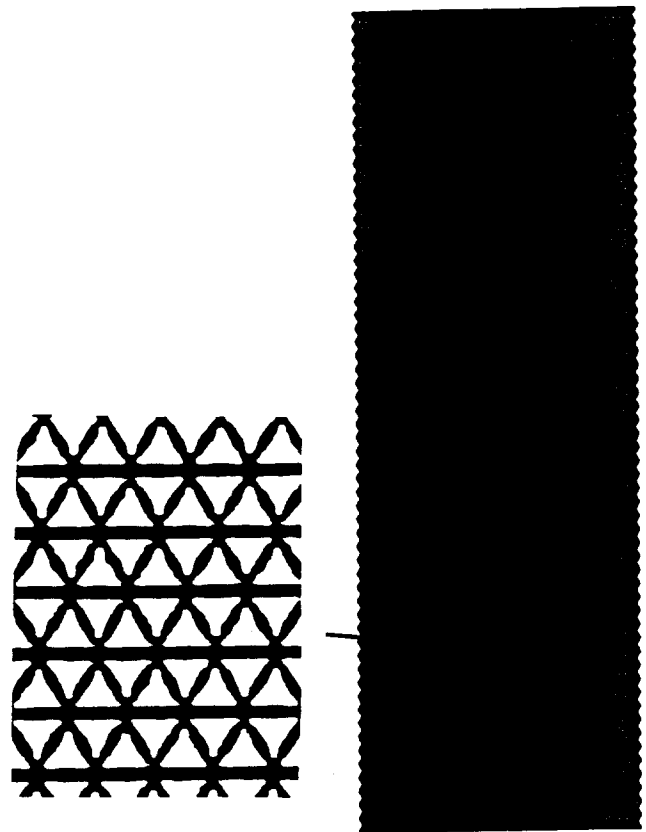


Fig. 4. A 40×120 triangular lattice.

During processing of a composite material, a 'reaction zone' is formed, i.e. an interface that may impart bonding between the matrix and the fiber.⁶ Several works have examined the material in the vicinity of the fiber, identifying significantly different properties than the matrix. That region is often called the mesophase.²⁷ Despite extensive work in this area, the behavior and properties of such a 'mesophase', or 'transition region' or 'interface' or 'interface reaction zone', have not been understood well.

The SCS-6 (SiC) fiber is approximately 140 μm in diameter. Its coating is $\sim 3 \mu\text{m}$ thick and has two layers of 1.7 and 1.3 μm thickness, respectively. Both these layers are composed of a turbostratic carbon matrix containing SiC particles and are separated by a very thin transition layer of carbon. In a composite made of titanium alloy matrix and SiC fiber with carbon coating a reaction zone consisting of several layers of Ti_xC_y and Ti_xSi_y is formed and is modulated by the alloying composition of the matrix and the processing procedure. Similar considerations hold for ceramic matrix composites. A thorough presentation on this subject can be found in Karpur *et al.*⁵ and the references cited there, where also the concept of the 'equivalent elastic interface' (EEI) is introduced. The concept is relevant to, and complements the present study; thus, the ideas behind the EEI are briefly described here. Since the thickness of the transition region (interface) and the spatial variation of properties along it are difficult to quantify, it is advisable to consider an equivalent homogeneous transition region — an interphase.

It is difficult to specify the exact thickness of the (homogeneous) transition region, and the analysis would be sensitive to changes in thickness. In order to overcome this difficulty, the properties of the interface can be defined in such a way that its response is independent of thickness. Thus interface properties should be defined in such a way that delivery of information, the jump in displacement and the transmitted stress across the interface, is consistently independent of thickness. This is accomplished precisely by dividing the relevant quantities — modulus of the homogenized region and failure stress — by the transition region thickness. For example, if S denotes the interface stiffness coefficient (elastic modulus E over thickness h), σ the normal stress at the interface, and u the jump displacement across the interface thickness, it is straightforward to show that $S = \sigma/u = E/h$. Thus, by defining quantities

such as the 'stiffness coefficient' and 'failure stress coefficient' (failure stress over thickness) the need for precise specification of the thickness is overcome.

It is feasible to measure such coefficients non-destructively, i.e. the 'shear stiffness coefficient' using the theoretical model developed by Matikas and Karpur²⁸ and Karpur *et al.*⁵ for the characterization of the interface, together with ultrasonic quantification. The present and next paragraph describe such a process, briefly. For the development of the theoretical model, the interface between the matrix and the fiber is modeled by (i) assuming continuity of normal and shear stresses and normal displacements at the interface, and (ii) allowing the discontinuity of shear displacements at the interface. It is assumed that the (ultrasonic) vibration is transmitted instantaneously from one medium to the other by weightless shear springs with an equivalent rigidity denoted as N_s (MPa/ μm). Since the interphase might generally have variable properties along its thickness, the shear modulus of the interphase zone and the shear stiffness coefficient (N_s) are integrals over the thickness and represent statistical average values. As a result, the shear stiffness coefficient of the interface is a measure of the shear stress transmitted across the equivalent elastic interface per unit of elastic differential displacement.

Ultrasonic quantification of the shear stiffness coefficient can be obtained by the measurement of the back-reflected ultrasonic shear waves from the fibers.²⁹ The incident stress wave induces a displacement of the matrix at the interface which is partially transmitted to the fiber due to the elastic deformation of the interphase region. The degree of discontinuity of the displacements and the associated partial transfer of stresses across the interface is a function of the interfacial shear stiffness coefficient. However, due to the conservation of energy requirements (continuity of stresses), the remaining part of the incident ultrasonic energy will be reflected back to the transducer. As a result, after experimentally measuring the incident and reflected ultrasonic energies, the part of the stress reflected from the fiber can be calculated as a percentage of the incident energy (back-reflection coefficient). This back-reflection coefficient is also a measure of the part of the stresses transmitted across the interface to the fiber because of the continuity of stresses at the interface. Therefore, the ultrasonic shear back-reflection coefficient can be used to calculate the shear stiffness coefficient of the interface by

simple inversion of the theoretical equation. It should be noted that the experimentally determined shear stiffness coefficient will be an average over the ultrasonic beam diameter (which is related to the incident wavelength) at the interface along the circumference of the fibers.

In our lattice discretization, the smallest discretization scale (the lattice spacings) is assigned to the interface thickness. Thus the interface is considered homogeneous by definition. A stiffness coefficient S and a failure stress coefficient F (failure stress over modulus) are assigned to it, and its failure is considered brittle. As mentioned previously the (shear) stiffness coefficient can be evaluated nondestructively. At this time the relevant experiments are being conducted²⁹ and correlations with the present study will be examined later. At this stage, the relevant interface properties will be deduced from the destructive experiments via back analysis and physical reasoning.

3.2 Simulation results

The following have been assumed in the numerical simulation procedure. Inertia effects and body forces are neglected, and load is applied slowly enough so that there is enough time for redistribution of stress before failure/yield proceeds further. The fiber, interface and ceramic matrix are considered brittle — when a bond fails its load is reduced to zero and the released load is redistributed by solving the problem again with the broken bond absent. The difference for ductile matrix bonds (metal matrix) is that after the yield stress has been reached the modulus is changed to the (linear) hardening modulus E_{mh} . Thus the simulation procedure involves the following steps: (a) discretize the structure into a lattice; (b) assign a failure/yield stress and stiffness to each bond, depending on whether it is spatially within matrix (brittle or ductile), fiber, or interface; (c) apply an increment of external displacement or load until the failure or yield criterion is satisfied by the bond carrying the maximum load — the problem being linear makes identification of that load easy; (d) if that bond is brittle, release the load carried by it, or if that bond is ductile apply the new modulus (E_{mh}) to it, and repeat this step if another bond fails during the process of load release; (e) increment the externally imposed boundary condition until the next bond fails or yields and repeat the previous step. Allowing failure or yield of one

bond at a time, together with the linearity of the problem during each step, assures a unique solution.

3.2.1 Simulation results — fragmentation test

The following properties for the fiber and matrix are considered and assigned to the corresponding lattice bonds.^{10,16} For the SiC (SCS-6) fiber a Young's modulus $E_f = 393$ GPa, and a failure stress $\sigma_f = 3.5$ GPa. Fiber failure is perfectly brittle — when a bond fails its load-carrying capacity is reduced to zero. The Ti-6Al-4V matrix is ductile, with a Young's modulus $E_m = 110$ GPa and yield stress $\sigma_m = 0.83$ GPa. For the linear hardening post-yield response the modulus is considered a fraction of E_m , i.e. $E_{mh} = E_m/100$. The dependence of the fiber fragmentation pattern on E_{mh} is examined in the following. The matrix is not allowed to fail — due to its ductility, failure occurs at large strains and the simulation is not carried out to such levels.

For identification of interface properties the following can be considered. We employ the experimental evidence that no fiber failure occurs in the linear regime of the specimen's stress–strain response (Fig. 1) but fiber failure initiates in the vicinity of the deviation from linearity. Having the matrix and fiber properties fixed, the interface properties have to be such that the predicted load–displacement response and fragmentation pattern match the experimental results as close as possible. These impose important restrictions on the properties of the interface. Thus, together with the (stepwise) linearity of the problem a few simulations can identify the range of interface properties. Before we identify such ranges, we present the conclusions from the simulations.

- (a) The fiber fragmentation pattern depends strongly on the volume of the matrix present. This has also been demonstrated experimentally.^{13,14} It can be better understood if we consider the following. In the limit case of very small or negligible matrix volume, a single fiber failure will occur. As the amount of matrix surrounding the fiber increases there should be a threshold where multiple fiber fragmentation occurs. By increasing the amount of matrix further, the result is reduction in the average fragmentation length. The saturation limit, if it exists, depends on the properties of the interface. Our analysis shows that the threshold for the present material combina-

tion is at a matrix–fiber ratio (in two dimensions) of approximately 10–12. A similar observation was made by Ochiai and Osamura¹⁴ in their experiments on W fiber/Cu matrix composites. They indicated that fiber fragmentation occurred till a maximum fiber volume fraction of ~ 10%. It is noted that in their experiments panels of rectangular cross-section were used, while our analysis is two-dimensional. This is discussed further in the sequence. The approximation (10–12) in our analysis is due to the following.

- (b) The matrix hardening modulus E_{mh} influences the fragmentation pattern. The influence is not sensitive — only large changes in E_{mh} influence the fragmentation pattern, i.e. average length between fragments. For $E_{mh} = 0$ a single fiber fracture occurs, or even no fiber fracture at all, depending on the interface properties.
- (c) Both the interface modulus and strength, and their relative values, influence the fragmentation pattern. A weak interface will fail even before the matrix yields, the result being that the fiber will simply act as an inclusion in the matrix. This also depends on the modulus. For example, if the interface and fiber are subjected to the same strain, the fiber will fail first only if the interface relative values (strength, modulus) allow so. Interface modulus does not have a strong effect within changes of about 100% or less.
- (d) The simulations showed that it is practically impossible to achieve fragmentation lengths (average) of the order of or lower than the fiber diameter. Perhaps this provides goals such as tailoring the interface properties. In passing, it is herein speculated that the optimum interface properties depend on the geometric and loading conditions of a specific test and/or configuration. For example if fibers are close together without ‘enough’ matrix material in between the optimum interface properties are possibly different than the ones implied by a single fiber fragmentation test. This important area seems to be totally unexplored. It is currently being addressed.
- (e) Immediately after the fiber breaks at some location, tension cracks propagate along the interface. In order for fragmentation to occur these cracks have to be arrested and

the arresting length (and thus the fragmentation pattern) are influenced strongly by the interface strength. This provides significant limitations to the range of interface strength. In other words, the debond length is important and should be measured, when possible, during the relevant testing.

- (f) The load–displacement or stress–strain response of the specimen is practically insensitive to the interface properties. This is mainly because the one fiber specimen does not behave as a composite. Thus the observed fragmentation pattern and debond length are the ones providing information on interface properties.

Figure 5 shows the load–displacement (stress–strain) response obtained from a 40×120 lattice. The material properties used for the matrix and fiber are the ones given above. For the interface the modulus coefficient derived is $857 \text{ MPa}/\mu\text{m}$ and the failure strength coefficient for one of them is $11 \text{ MPa}/\mu\text{m}$ and of the other one $6 \text{ MPa}/\mu\text{m}$. The meaning of such interface properties is discussed below. The (small) stress drops in the curves correspond to successive fiber breaks. It is noted that experimentally, often, no load drop is observed, for example Ochiai and Osamura¹⁴ observed them, while Roman *et al.*¹⁰ did not. Since it is known that the fiber breaks at those levels of stress, no load drop may be attributed to small snap-through, to rate of loading effects, or to the sensitivity of the equipment used. The predicted stress–strain response (Fig. 5) correlates well with the experimental one (Fig. 1(b)) where yield initiates at about 850 MPa, at a strain close to the 2% level. Further it is noted that with these values for the interface properties most of the matrix yields before fiber breaks initiate.

The simulation is two-dimensional while the actual fragmentation test (Fig. 1) is three-dimensional! The diameter of the SiC fibers is approximately 0.14 mm. The samples¹⁰ were 1.50 mm thick, 19.05 mm (gage) long and 6.53 mm wide in the gage section. Thus the problem is not axisymmetric. It was mentioned that the fragmentation pattern depends on the amount of matrix surrounding the fiber. In the three-dimensional case it is not clear if the minimum matrix dimension (1.50 mm for the tests) or the area of the matrix ($1.50 \times 6.35 \text{ mm}^2$) or both are decisive with respect to the fragmentation pattern. For the test configuration, the ratio (matrix/fiber) with respect

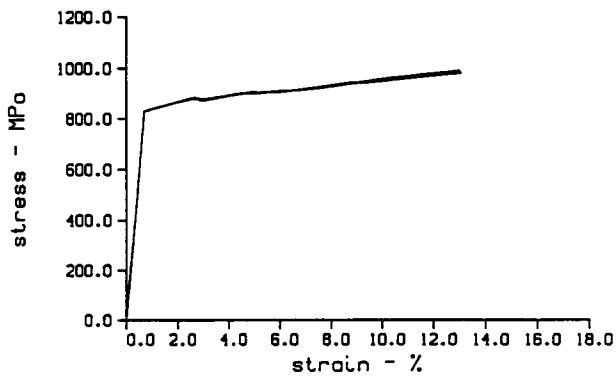


Fig. 5. Two, apparently indistinguishable, stress-strain responses obtained with identical material properties except the interface strength coefficient, $F=11$ MPa/ μm and $F=6$ MPa/ μm .

to the minimum dimension is approximately 1.5/0.14. Experimentally this ratio seems to govern the fragmentation pattern rather than the cross-sectional area ratio. Three-dimensional simulations are not attempted at this time, due to excessive computer time requirements. Further, several issues need to be understood before three-dimensional effects come into the picture.

Although the two different values for the interface strength coefficient yielded a similar load-deformation response, the fragmentation patterns that evolved were different. In the following figures, for effective presentation, a broken bar is represented by a thin, short line perpendicular to it. Figure 6 shows some of the evolution stages of fiber fragmentation and interface failure for $S=11$ MPa/ μm , and Fig. 7 shows some of the stages for $S=6$ MPa/ μm . The following have been identified:

- (1) Interface cracks at the fiber ends initiate and quickly become arrested. This is consistent with the analysis and experiments by Atkinson *et al.*¹⁹ on the stability of interface cracks near the fiber end, for an embedded fiber.
- (2) For both cases the fiber breaks first in the middle of its length. The reason why this happens is explained subsequently.
- (3) After, or concurrently with, the first full fiber crack development (over its width) cracks propagate along the interface and at some point are arrested: Figs 6(b) and 7(b).
- (4) The crack length along the interfaces is important with respect to subsequent fiber breaks, and thus with respect to the final

fragmentation pattern. If Figs 6 and 7 are compared, it is seen that the interface crack length is smaller in Fig. 6 than in Fig. 7. This is the decisive reason for the final fragmentation pattern. In Fig. 6 the average fragmentation length is about half that in Fig. 7.

- (5) The differences between Figs 6 and 7 can be explained by the length of interface cracks. In Fig. 6, for example, a greater total length of interface is required to transmit enough load to the fiber — capable to break it. The interface strength is important here. Figure 8 shows the crack evolution when an interface strength coefficient $F=1$ MPa/ μm is considered, the other parameters being the same as these used for Figs 6 and 7. For strengths even lower than that, no fiber breakage is observed.
- (6) The fragmentation spacing is not constant (a distribution of fragment lengths develops) for the following reasons: (a) after the first break occurs in the middle (as explained in the next paragraph), i.e. Fig. 6(a) and (b), stress distribution in the upper and lower halves of the fiber ceases to be symmetric and thus the next fiber break may not occur at a quarter of the fiber length; (b) in the algorithm, when the fracture criterion is met by two (or more) bars simultaneously, only one of them is actually broken and the system is re-equilibrated. This may suspend the symmetry of the problem from the early straining stages, i.e. note the (small) cracks at the top of Fig. 6(a).

So now the question of why the first fiber break develops in the middle comes into the picture. We find this opportunity to discuss further, and at the same time, the problem of the ratio of the width of the sample (or matrix) to the diameter of the fiber. Let us reduce the amount of matrix surrounding the fiber, say a lattice of 30×120 with the same dimensions for the fiber as before. For interface properties identical to those that produced Fig. 6, a single fiber break will develop (no fragmentation) for his 30×120 configuration. Let us look at the distribution of strain before fiber fracture. Figure 9 shows the distribution and is plotted as follows. Only bonds exceeding a certain level of strain are drawn. Clearly the stress concentration is in the middle. In order for the fiber to break, enough load to cause this must be built up in the

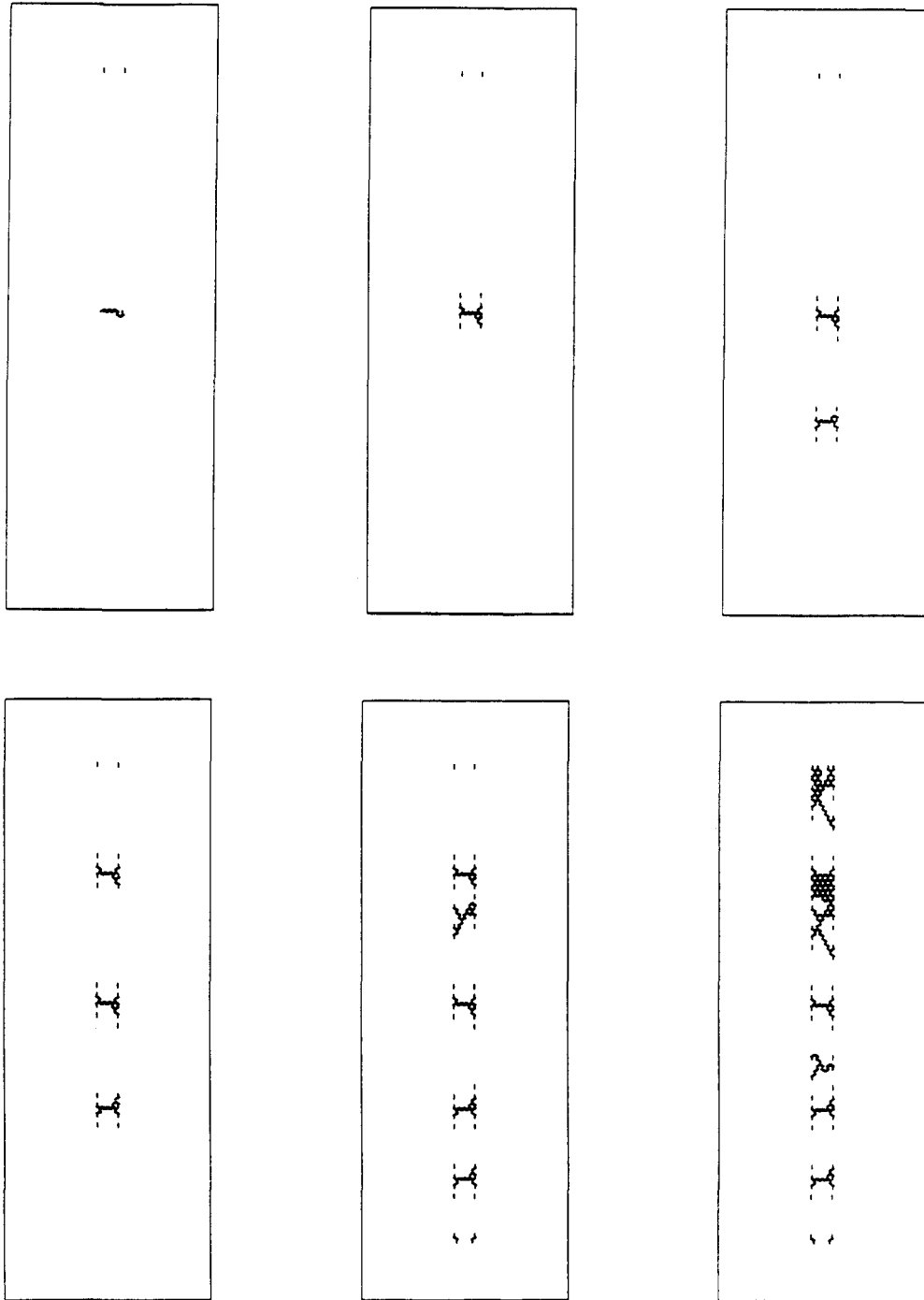


Fig. 6. Fiber fragmentation and interface failure stages for interface strength coefficient $F = 11 \text{ MPa}/\mu\text{m}$.

matrix and the interface must be capable of transmitting the force to the fiber. For the present fiber, matrix and interface properties, the horizontal dimension of 30 units is approximately the lower limit over which this will happen.

The interface region is considered homogeneous. This, of course, is an approximation of the reality. In general, at the micro-level (at the length

scale of a material's microstructure) it may be argued that failure is predominantly in tension. Then, compressive failure is the integrated, phenomenological combination of several tensile micro-failures. By considering the interface as being homogeneous, we indirectly imply or assume that the actual response is homogenizable. Then failure in compression is possible. For the

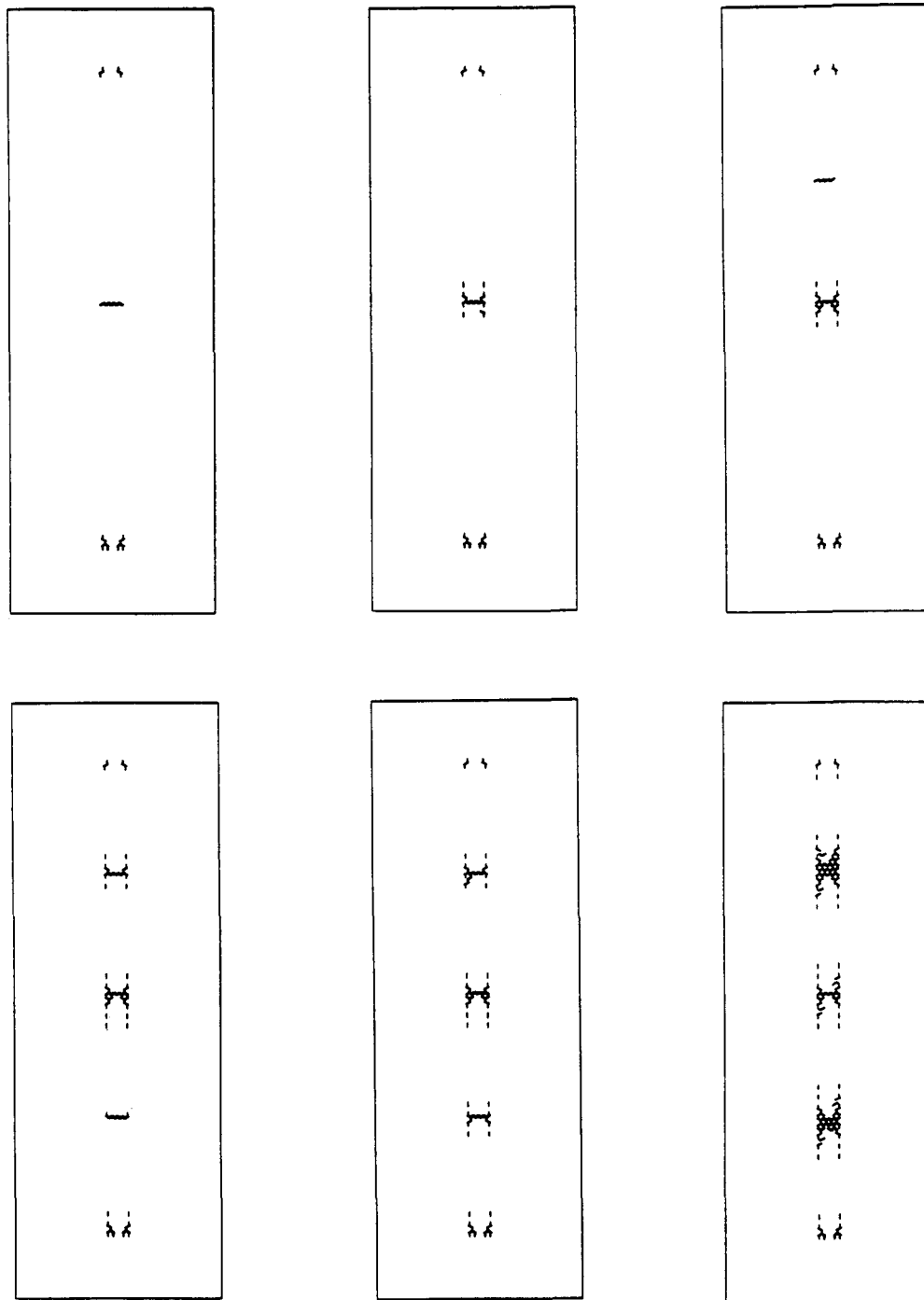


Fig. 7. Fiber fragmentation and interface failure stages for interface strength coefficient $F=6 \text{ MPa}/\mu\text{m}$.

single fiber fragmentation test, compressive failure proved unimportant. However, for the push-out and pullout tests, not allowing compressive failure introduces regions where failure is 'prohibited'. Then, due to the homogenization assumption, interface compressive failure should be considered. An effective procedure for identifying differences between tensile and compressive

failure would be by comparing reversed tests, i.e. pushout and pullout. Comparison of the load levels that initiate micro-fracturing should provide the relevant information, since after micro-crack initiation the problem is nonlinear. Such experimental information is not available at this time. However, our back-analysis of simulation results showed that a ratio of compressive to tensile

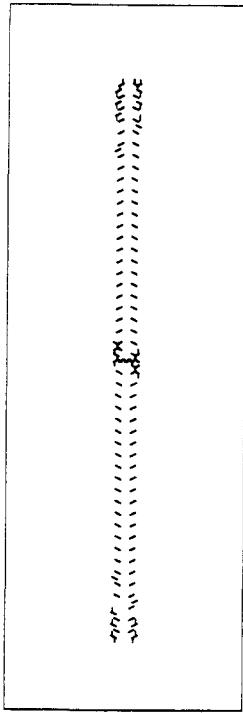


Fig. 8. Crack pattern for interface strength coefficient $F=1 \text{ MPa}/\mu\text{m}$.

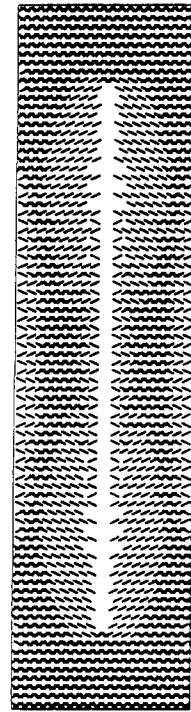


Fig. 9. Strain distribution before fiber fracture.

failure stress of five provides a reasonable estimate. The effect of that ratio is examined subsequently.

3.2.2 Simulation results — pushout/pullout, metal matrix

The pushout and pullout tests on metal matrix composites are usually performed on thin specimens sliced perpendicular to the fiber axis.^{17,18,30} Interface properties are (usually) extracted from such tests by considering the average shear stress at the interface (external load over interface area). The ratio of specimen at height over fiber diameter ranges between 1.0 and 3.4. Specimens are mounted on a support block which has a groove (sometimes a hole) two to four fiber diameters wide. The purpose of the groove is to allow the fiber to be pushed out. Since the recess in the support surface is typically a linear groove, axial symmetry of the problem is lost. Figure 10 shows schematically the sequence of events and stress distribution during the pushout test.^{17,18} Our simulations agree with some of the conclusions made in that paper. Additional, important points are presented below.

For simulation of the pushout/pullout tests, a 120×25 lattice is considered. The fiber is eight lattice units wide (diameter) and 25 units in height. Thus the height over diameter ratio is 3.125. As

previously, the interface thickness is one lattice unit. Since the specimen's height is relatively low (especially when compared to the heights used in ceramic matrix composites examined in the next section) two sample support configurations were examined. In the first one the support 'hole' is 1.25 times the fiber diameter, while in the second one it is 2.75 times. The fiber, matrix and interface properties are those used for simulating the fragmentation test (see above) with $S=11 \text{ MPa}/\mu\text{m}$. The simulations showed the following:

- (1) Even for relatively low imposed external displacement, small, stable cracks form at the interface near the external load application side (at the top), for both the pushout and pullout cases. These cracks have no apparent implications on the load-displacement curve of the simulation.
- (2) After the arrest of the cracks mentioned above, tension and shear dominated interface cracks initiate at the side opposite to the external load application. These cracks are initially unstable and result in a noticeable drop in the external load. Such cracks form in both the pullout and pushout cases. The reason for such cracks is intense free surface effects at the bottom end of the fiber, with bending of the unsupported matrix for the pushout case, and Poisson effects for the pullout case.

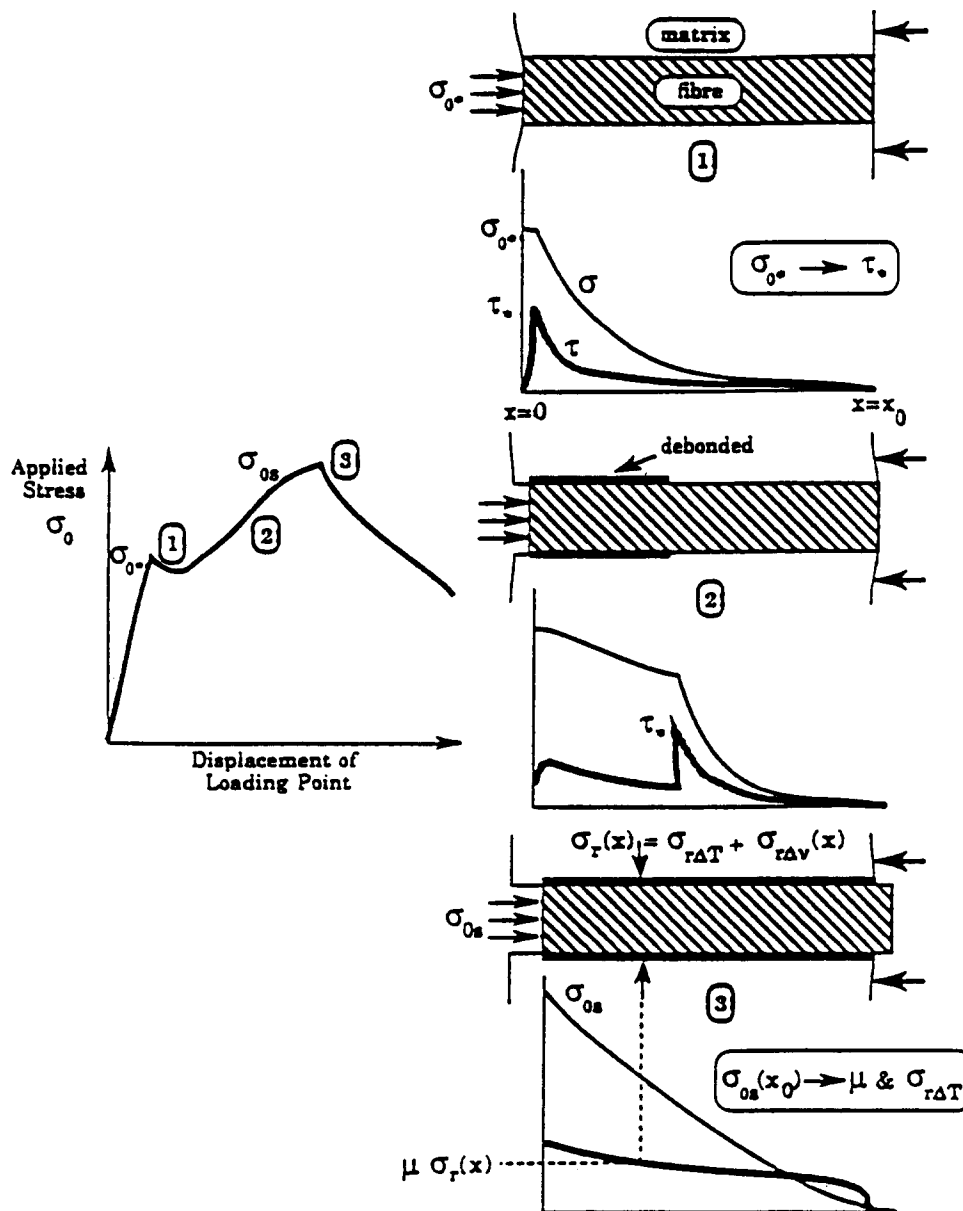


Fig. 10. Schematic illustration of events and stress distribution during the pushout test. From Watson and Clyne.¹⁷

- (3) After the arrest of the cracks that initiated at the bottom, further external load is required for the whole interface to fail.
- (4) Pushout requires a larger load than pullout. This is attributed mainly to Poisson effects that tend to either stabilize or destabilize interface crack propagation, together with differences in failure due to tension and compression. The ratio of failure stress in compression over failure stress in tension in these simulations is five.
- (5) The size of the 'hole' at the bottom support has a significant effect on the load-deformation response. This is mainly due to the

small thickness of the sample. For large thicknesses this effect is not present, as will be discussed in the next section for ceramic matrix composites.

- (6) The effects of residual stress, although not examined herein, seem to be important — this is concluded from the fact that during the pushout/pullout process the matrix near the interface is in the regime of yield initiation, and partial small-scale yielding occurs. The residual stresses are expected to influence these trends and thus the overall load-deformation response. Residual stresses can be quite high in metal matrix

composites.³¹ Their influence is currently being studied.

Figure 11(a) and (b) shows the predicted load–displacement curves for bottom ‘hole’ to fiber diameter ratios of 1.25 and 2.75, respectively. It is seen that the larger hole shows a decrease in peak load by as much as 20% over the smaller one.

In general, the results compare well with the reported experimental results.^{17,18,30} The results herein correspond to the Ti–6Al–4V matrix, which forms a ‘good’ interface with the SCS-6 as compared to other Ti-based matrices. For the large (2.75 × fiber diameter) opening at the bottom case the average shear stress (load over interface area) at (global) peak load is approximately 250 MPa for pushout and 150 MPa for pullout. Factors that influence these values are the geometry of the problem, i.e. opening at the support, specimen thickness, and the residual stresses that are not examined herein. If such stresses result in significant matrix yielding during the tests, then the peak loads are expected to be smaller than those in Fig. 11 and the corresponding displacements larger. It is not known how three-dimensional effects, i.e. the non-circular opening at the support system used in the experiments, non-uniform interface failure along the fiber circumference (localization), etc., influence the experimental data or the simulation procedure. Figure 12 shows the interface crack patterns

at a stage of loading for the pullout and pushout simulation (load imposed on the left side). It is important to note that the interface properties used for the prediction of the pushout/pullout tests are those evaluated from the back-analysis of the fragmentation test results. One of the issues not resolved is the influence of the amount of matrix material in the fragmentation tests, since the setup is not axisymmetric. The ‘mapping’ to two dimensions was done, herein, with respect to the minimum specimen thickness. The influence of the third dimension is not clear at this point.

3.2.3 Simulation results – pushout/pullout, ceramic matrix

The pushout/pullout test setup for ceramic matrix materials is similar to those described above with the following differences: the matrix is brittle, the specimen thickness is much larger, and the interface is much weaker (residual stresses are discussed later and are not included in the present analysis). For the simulations the same fiber properties (SCS-6) are considered. For the glass matrix $E_m = 65$ GPa and brittle failure occurs at $\sigma_t = 0.1$ GPa. Typically the specimen thickness is about 20 times the fiber diameter. In the simulations we consider a 40×40 lattice, the fiber being 2×40 and, as before, the interface is one lattice spacing wide. For identification of the interface properties, we employ the experimental evidence

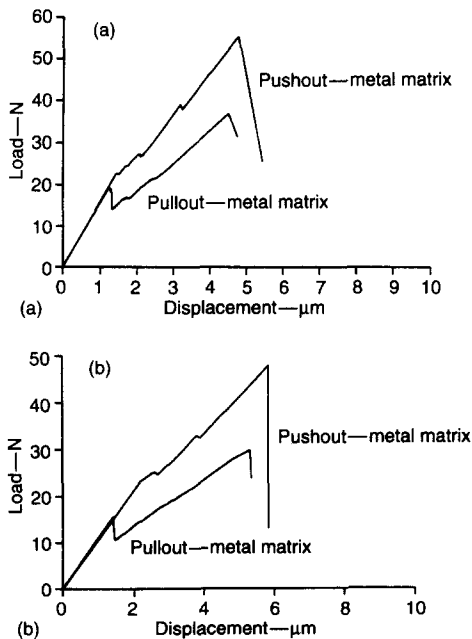


Fig. 11. Load–displacement curves for different bottom support openings: opening/fiber diameter = (a) 1.25, (b) 2.75.

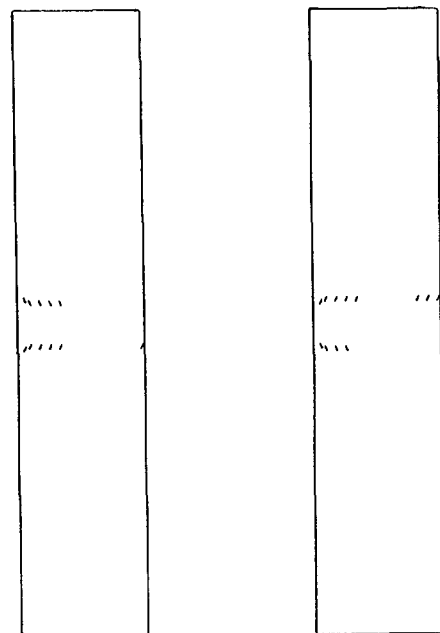


Fig. 12. Crack patterns for the pullout, pushout tests after the (first) load drop (Fig. 10).

that during the pullout/pushout process, no damage is induced on the matrix or the fiber. The simulations showed the following, comparing the present cases (ceramic matrix) with the previous ones (metal matrix):

- (1) Since interface properties that would induce matrix damage were not considered, the matrix remains in its elastic regime (below its failure stress) throughout the entire pullout/pushout process. Then, it is mostly the geometry of the problem, together with the interface properties, that dominate the response.
- (2) The size of the 'hole' at the bottom of the specimen has practically no influence on the load-displacement and crack pattern predicted through simulation. The results presented in the following were obtained with an opening at the bottom equal to three times the fiber diameter.
- (3) Contrary to the metal matrix cases, no significant cracking initiated at the bottom.

Figure 13 shows the load-displacement response predicted with a stiffness coefficient $S=70 \text{ MPa}/\mu\text{m}$ and a failure stress coefficient $F=0.09 \text{ MPa}/\mu\text{m}$. As before the ratio of compressive over tensile failure stress is considered equal to five. Figure 14 shows the crack patterns obtained at various stages of applied load. Figure 15 shows the influence of S and of the ratio of compressive over tensile failure stress (when compared with Fig. 13) on the load-displacement response. These curves can be directly compared with experimental/analytical data — together with statistical analysis of the data scatter, not considered herein, reliable values of the homogenized interface properties can be obtained.

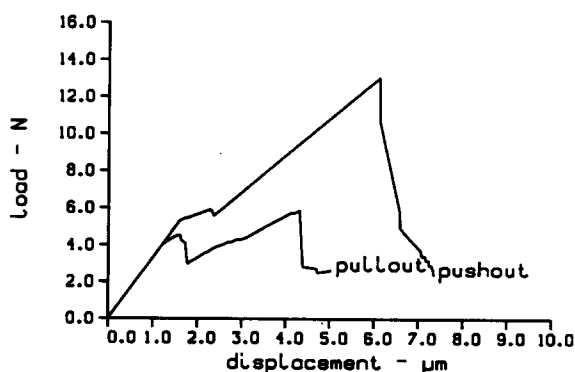


Fig. 13. Load-displacement response for fiber pushout, pullout in glass matrix. $S=70 \text{ MPa}/\mu\text{m}$, $F=0.09 \text{ MPa}/\mu\text{m}$.

4 DISCUSSION AND CONCLUSION

The present analysis has been based on the homogeneous interface region assumption. It may be, however, that homogenization of the actual interface response is not possible or reasonable. For

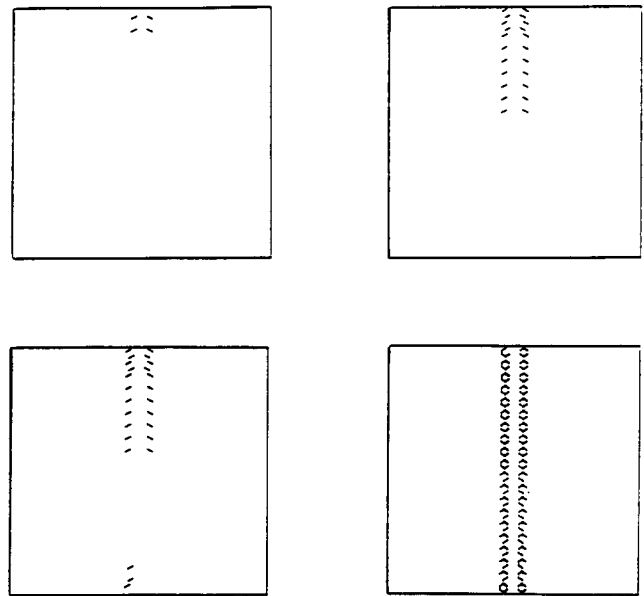


Fig. 14. Crack patterns for pushout, at various stages of loading.

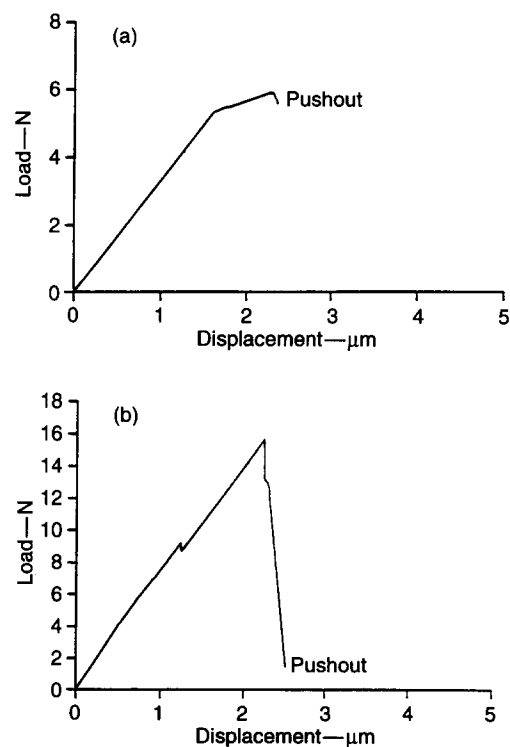


Fig. 15. Simulated load-displacement response: (a) $S=15 \text{ MPa}/\mu\text{m}$, $F=0.09 \text{ MPa}/\mu\text{m}$, ratio of compressive/tensile failure stress = 10; (b) $S=140 \text{ MPa}/\mu\text{m}$, $F=0.09 \text{ MPa}/\mu\text{m}$, ratio of compressive/tensile failure stress = 10.

example, typically, heterogeneous materials develop a disordered network of micro-cracks from the early straining stages. For strain levels beyond a relatively low threshold, homogenization is only possible for large length scales, much larger than the initial (at zero straining) heterogeneity scale of the material. Experimental evidence³² for metal matrix composites shows development of localized interface damage, under even very low strain levels. Thus, if this is the case, the interface properties obtained herein by back-analysis do not represent actual local properties. Perhaps the best way to obtain local properties is through nondestructive evaluation.⁵ Several questions, about the 'evolution' (with straining) of such properties and about homogenization (if possible) based on rigorous analysis, have yet to be examined. From this perspective, the present study is only a first attempt towards understanding interface response and its influence on composite material performance.

Residual stresses in metal matrix composites are relatively large.³¹ Even in metal matrix composites they can be important. By ignoring them in the present analysis, we are not able to separate the effect of residual stresses from the 'actual' interface response. Thus, especially for quantitative evaluation of interface parameters, the present work is amendable to incorporation of residual stress, for both metal matrix and ceramic matrix tests. This important issue is currently being addressed analytically and experimentally. Another issue concerns friction and interface roughness,³³ which affect the load-carrying ability of the interface after debonding. It is possible to incorporate such effects in the present analysis by altering the post-peak response of the (homogenized) interface. We feel that this is closely related to residual stresses and has yet to be examined.

ACKNOWLEDGEMENTS

This work was supported by the Air Force Office of Scientific Research (AFOSR/RDL/SFRP/93-149 to GNF), the National Science Foundation (NSF/PYI/MSS-9157237 to GNF) and by Materials Directorate, Wright Laboratory, Wright-Patterson Air Force Base, Ohio 45433, Contact Nos F33615-89-C-5612 to PK and F33615-92-C-5663 to SK. Discussions with B. Majumdar, D. Miracle, T. Nicholas and N. Pagano have been very fruitful.

REFERENCES

1. Kerans, R. J., Hay, R. S., Pagano, N. J. & Parthasarathy, T. A., The role of the fiber-matrix interface in ceramic composites. *Am. Ceram. Soc. Bull.*, **68** (2) (1989) 429-42.
2. Evans, A. G. & Marshall, D. B., The mechanical behavior of ceramic matrix composites. *Acta Metall. Mater.*, **37** (10) (1989) 2567-83.
3. Jero, P. D., Kerans, R. J. & Parthasarathy, T. A., Effect of interfacial roughness on the frictional stress measured using pushout tests. *J. Am. Ceram. Soc.*, **74** (11) (1991) 2793-801.
4. Parthasarathy, T. A., Jero, P. D. & Kerans, R. J., Extraction of interface properties from fiber push-out test. *Scripta Metall. Mater.*, **25** (1991) 2457-62.
5. Karpur, P., Matikas, T. & Krishnamurthy, S., A novel parameter to characterize the fiber-matrix interphase/interface for mechanics of continuous fiber reinforced metal matrix and ceramic matrix composites. *Comp. Sci. Tech.*, (under review).
6. Metcalfe, A. G., *Interfaces in Metal Matrix Composites*. Academic Press, New York, 1974.
7. Evans, A. G., Zok, F. W. & Davis, J., The role of interfaces in fiber-reinforced brittle matrix composites. *Comp. Sci. Tech.*, **42** (1991) 3-24.
8. McCartney, L. N., New theoretical model of stress transfer between fibre and matrix in a uniaxially fibre-reinforced composite. *Proc. Roy. Soc. London. A* (1990) 425-42.
9. Pagano, N., Axisymmetric micromechanical stress fields in composites. In *Local Mechanics Concepts for Composite Material Systems*, ed. J. N. Reddy & K. L. Reifsnider, 1991.
10. Roman, I., Krishnamurthy, S. & Miracle, D. B., Fiber-matrix interfacial behavior in SiC-titanium alloy composites. 1993 (preprint).
11. Karpur, P., Matikas, T., Krishnamurthy, S. & Ashbaugh, N., Ultrasound for fiber fragmentation size determination to characterize load transfer behavior of matrix-fiber interface in metal matrix composites. In *Review of Progress in Quantitative NDE*, La Jolla, CA, 1992.
12. Karpur, P., Matikas, T. E. & Krishnamurthy, S., Matrix-fiber interface characterization in metal matrix composites using ultrasonic imaging of fiber fragmentation. *American Society for Composites*, (1992) 420-9.
13. Kelly, A. & Tyson, W. R., Tensile properties of fiber-reinforced metals: Cu-W and Cu-Mo. *J. Mech. Phys. Solids*, **13** (1965) 329-50.
14. Ochiai, S. & Osamura, K., Stress distribution of a segmented fibre in loaded single fibre-metal matrix composites. *Z. Metallkunde*, **77** (1986) 249-54.
15. Ochiai, S. & Osamura, K., Multiple fracture of a fibre in a single tungsten fibre-copper matrix composite. *Z. Metallkunde*, **77** (1986) 255-9.
16. Kerans, R. J. & Parthasarathy, T. A., Theoretical analysis of the fibre pullout and pushout tests. *J. Am. Ceram. Soc.*, **74** (1991) 1585-96.
17. Watson, M. C. & Clyne, T. W., The use of single fibre pushout testing to explore interfacial mechanics in SiC monofilament-reinforced Ti-I. A photoelastic study of the test. *Acta Metall. Mater.*, **40** (1992) 131-9.
18. Watson, M. C. & Clyne, T. W., The use of single fibre pushout testing to explore interfacial mechanics in SiC monofilament-reinforced Ti-II. Application of the test to composite materials. *Acta Metall. Mater.*, **40** (1992) 141-8.

19. Atkinson, C., Avila, J., Betz, E. & Smelser, R. E., The rod pull out problem, theory and experiment. *J. Mech. Phys. Solids*, **30** (1982) 97–120.
20. Hrennikoff, A., Solution of problems of elasticity by the framework method. *J. Appl. Mech. ASME, A* (1941) 169–75.
21. Herrmann, H. J. & Roux, S., (eds). *Statistical Models for the Fracture of Disordered Media*. North-Holland, Amsterdam, 1990.
22. Charmet, J. C., Roux, S. & Guyon, E. (eds), *Disorder and Fracture*. Plenum Press, New York, 1990.
23. Schlangen, E. & van Mier, J. G. M., Simple lattice model for numerical simulation of fracture of concrete materials and structures. *Mater. & Struct.*, **25** (1992) 534–42.
24. Murat, M., Anholt, M. & Wagner, H. D., Fracture behavior of short-fibre reinforced materials. *J. Mater. Res.*, **7** (1992) 3120–31.
25. Monette, A. G., Anderson, M. P., Ling, S. & Grest, G. S., Effect of modulus and cohesive energy on critical fibre length in fibre-reinforced composites. *J. Mater. Sci.*, **27** (1992) 4393–405.
26. Dai, H. & Frantziskonis, G., Heterogeneity, spatial correlations, size effects and dissipated energy in brittle materials. *Mech. of Mats.*, (preprint).
27. Theocaris, P. S., *The Mesophase Concept in Composites*. Springer-Verlag, New York, 1987.
28. Matikas, T. & Karpur, P., Ultrasonic reflectivity technique for the characterization of fiber-matrix interface in metal matrix composites. *J. Appl. Phys.*, **74** (1993) 228–36.
29. Matikas, T. E. & Karpur, P., Micro-mechanics approach to characterize interfaces in metal and ceramic matrix composites. In *Review of Progress in Quantitative NDE*, Brunswick, ME, 1993.
30. Eldridge, J. I., Fiber pushout testing of intermetallic matrix composites at elevated temperatures. In *Materials Research Society Symposium*, 1992.
31. Coker, D., Ashbough, N. E. & Nicholas, T., Residual stresses in metal matrix composites. In *ASTM Symposium on Thermomechanical Fatigue Behavior of Materials*, San Diego, CA, 1991.
32. Majumdar, B. S., Newaz, G. M. & Ellis, J. R., Evolution of damage and plasticity in titanium-based, fiber-reinforced composites. *Metall. Trans.*, **24A** (1993) 1593–7.
33. Jero, P. D. & Kerans, R. J., The contribution of interfacial roughness to sliding friction of ceramic fibers in a glass matrix. *Scripta Metall. Mater.*, **24** (1990) 2315–18.